2014 IEEE International Conference on Robotics & Automation (ICRA)
Hong Kong Convention and Exhibition Center
May 31 - June 7, 2014. Hong Kong, China

Active Bending Motion of Pole Vault Robot to Improve Reachable Height

Toshihiko Fukushima[1], Satoshi Nishikawa[2] and Yasuo Kuniyoshi[3]

***Abstract*— For robots using elastic devices, pole vault is a particularly interesting task because poles have large differences from previously studied elastic elements in terms of their elastic capacity. The active actuation of the agent in "pole support phase" plays important roles in improving vaulting performance. Investigating this actuation can contribute to the design of novel control strategies during the time when the agent contacts with environment through the elastic device. In this study, we specifically examined an active bending effect performed in the "pole support phase." We analyzed the active bending effect on reachable height (vaulting height) using the "Transitional Buckling Model." We applied this active bending theory to a robot and verified the active bending effect to improve vaulting height. Results show that active bending motion in the "pole support phase" improves the pole vault performance and that the timing of the bending direction change is an important factor for defining the vaulting performance. These results will facilitate the application of robots using large elasticity.**

I. INTRODUCTION

To achieve dynamic robotic locomotion, the use of elastic elements has been examined since early times. Introducing air springs into the leg design enabled us to develop successful hopping and running robots [1], [2]. Coil springs were also used for energy regeneration of locomotion [3], [4]. Elastic blades have enabled robots to achieve a good power–weight ratio [5].

To improve locomotive performance further, elastic devices with extra-large elastic capacity will be needed. In one example, pole vaulting is a particularly interesting task. In pole vaulting, the pole dynamically converts horizontal velocity to vertical height. Humans can reach more than 6 m height using an elastic pole.

This large elastic capacity gives robots adequate duration of a "pole support phase" when robots are suspended from the pole. The "pole support phase" is defined as a phase between take-off from the ground and pole-release to free flight. Differently from the case of previous elastic elements, this "pole support phase" gives them an adequate time to actuate the elastic pole to improve the performance. Therefore, investigating actuation in such phases contributes to robotics in the novel design of the control strategy during the time when robots contacts with environment through the elastic device.

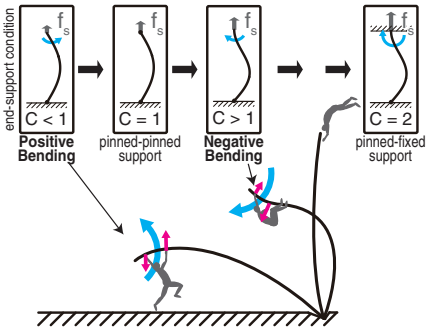

Fig. 1. Transitional Buckling Model. Pink linear arrows show forces from the arms. Blue curved arrows are input bending moments from arm forces.

In sport biomechanics, well-trained athletes are known to move actively in the "pole support phase." In fact, the athlete's total energy when crossing over the bar can exceed 120% of the initial energy at take-off from the ground [6]. This additional 20% energy stems from the athlete's motion in the "pole support phase." Many previous studies have measured athletes' motions in the "pole support phase." For example, Frère *et al.* examined electromyograms (EMG) of the muscles of the upper limbs and analyzed the role of each muscle [6]. Other studies such as that reported by McGinnis *et al.* have used inverse kinematics to calculate the moment exerted by the athlete [7]. These studies have specifically examined measurements reflecting the athletes' behavior.

However, they have not explicitly addressed the effect of the athlete's motion on the whole of the pole vaulting system. How the motion improves their vaulting height remains unclear. For elucidate these effects, we analyzed the active bending effect on vaulting performance in simulation experiments by the proposition of the Transitional Buckling Model [8]. This proposed model accounts for the athlete's active bending on the pole. Although the results of our previous work have suggested the effectiveness of active bending in numerical simulation, verification of the theory must be done in the real world to apply the theory to robots. As described in this paper, first, we briefly explain the theory and model of active bending effect and the simulation experiment. Next, we design a robot that can actuate the pole actively. Then we conduct robot experiments to verify the active bending effect. Finally, we discuss the application of active bending theory for robots using other elastic devices.

*This work was supported by Kakenhi No.22240015.

[1]Toshihiko Fukushima is with Graduate School of Interdisciplinary Information Studies, The University of Tokyo, Tokyo, Japan. fukushima@isi.imi.i.u-tokyo.ac.jp

[2]Satoshi Nishikawa, with the Graduate School of Information Science and Technology, The University of Tokyo, Tokyo, Japan, is a research fellow of Japan Society for the Promotion of Science. nisikawa@isi.imi.i.u-tokyo.ac.jp

[3]Yasuo Kuniyoshi is with Graduate School of Information Science and Technology, The University of Tokyo, Tokyo, Japan. kuniyoshi@isi.imi.i.u-tokyo.ac.jp

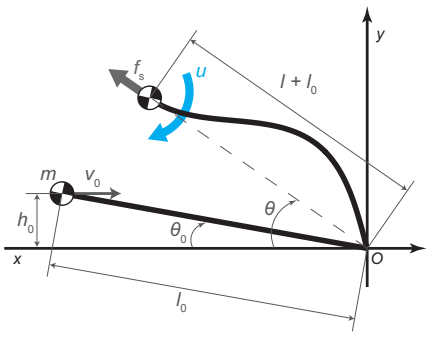

Fig. 2. Pole-suspended one-point mass model.

II. Model for Active Bending Effect

A. Active Bending Theory

According to previous works analyzing athlete's motion, by measuring EMG signals from upper limbs [6] and by solving inverse kinematics [7], a well-trained athlete bends the pole as follows (Fig. 1) [8].

Phase 1: Pole-deflecting phase
: By applying an upward force on the lower hand grip of the pole, the athlete bends the pole to increase pole deflection. Intuitively, the pole becomes more flexible and easier to deflect. Therefore, the pole stores more potential energy.

Phase 2: Pole-straightening phase
: By attracting the body to the pole and conducting an inversion, the athlete bends the pole to decrease pole deflection. Intuitively, the pole becomes stiffer and more difficult to deflect. Therefore the pole exerts a greater restoring force for the athletes to vault higher.

In summary, the athlete's motion generates a bending moment to transition the virtual stiffness of the pole.

B. Previous Pole Vault Model

First, we modeled the whole pole vault movement without an active bending effect. Behavior of a flexible pole has usually been analyzed using the Euler buckling model [9], [10]. The Euler buckling model treats the force exerted by the pole as a simple constant force. We modeled pole vault movement using this simplified model and treated an athlete as a mass point (Fig. 2). The equation of motion is represented as shown below.

$$\frac{d}{dt}\begin{pmatrix}\theta\\ \dot{\theta}\\ l\\ \dot{l}\end{pmatrix} = \begin{pmatrix}\dot{\theta}\\ -\frac{1}{l+l_0}(2\dot{l}\dot{\theta}+g\cos\theta)\\ \dot{l}\\ -(l+l_0)\dot{\theta}^2+g\sin\theta\end{pmatrix} + \begin{pmatrix}0\\ 0\\ 0\\ \frac{f_s}{m}\end{pmatrix}, \quad (1)$$

$$\text{where} \quad f_s = C\frac{\pi^2 EI}{l_0^2} = (\text{const.}). \quad (2)$$

Here, C is the end-support condition coefficient, E stands for the Young's modulus, and I is the area moment of inertia. The mass point has an initial horizontal velocity v_0. The pole applies the exerted force f_s on the mass point. The exerted force f_s can be represented by the Euler buckling load. According to the Euler buckling model, as long as the end-support condition of the pole remains constant, f_s remains constant irrespective of pole deformation. In the Euler buckling model, coefficient C is determined by the end-support condition (Fig. 1). Previous studies have not accounted for the active bending effect. They treated both the top and bottom end of the pole as pinned support. C was usually set to a constant value as $C = 1$ [9], [10].

C. Transitional Buckling Model

Next, we represent the active bending effect presented in Sec. II-A as the extended Euler buckling model. Our proposed model also treats the bottom end of the pole as pinned support, but it treats the top end of the pole differently as variable support transitioning according to a function of input bending moment u (Fig. 1). Consequently, by redefining the coefficient C as variable $C = C(u)$, we propose the Transitional Buckling Model (TBM), which can account for the active bending effect (Eq. (1), Eq. (3)) [8].

$$f_s' = C(u)\frac{\pi^2 EI}{l_0^2}. \quad (3)$$

The relation between active bending and $C(u)$ is the following.

Phase 1: $C(u) < 1$, Positive Bending
: Intuitively, a value which is comparable to the spring constant is small. The force received from the pole f_s' is small. Therefore, the mass point can deflect the pole with smaller force than in $C = 1$.

Phase 2: $C(u) > 1$, Negative Bending
: Intuitively, a value which is comparable to the spring constant is large. The force received from the pole f_s' is large. Therefore, the mass point can receive larger energy than in $C = 1$.

III. Simulation Experiments

We specifically examined the advantage of the input bending moment. To compare that, we conducted the following experiments. First, we experimentally compared the original buckling model treating C as constant (Non-actuation) and the TBM treating $C(u)$ as variable (Active-bending). Next, in the TBM, we experimentally explored the vaulting performance, shifting the timing and speed of change of the bending direction.

A. Experimental Setup

We simulated the pole vault by numerically solving ordinary differential Eq. (1) with a time step of 1 [ms]. Simulation parameters were determined by referring to an actual athlete's data (Table I). The mass point releases the pole when the pole straightens. Consequently, it takes off in a projectile motion. Vaulting height H_V is defined as the maximum height of the mass point in the projectile motion assuming the velocity which mass point had at the pole release time as an initial velocity.

TABLE I

SIMULATION PARAMETER

parameter	description	ex1	ex2
θ	elevation angle of mass	variable	$\rightarrow$
l	displacement from pole length	variable	$\rightarrow$
θ_0	initial pole angle	$\sin^{-1}(l/h_0)$	$\rightarrow$
l_0	pole length	3–5 [m]	$\rightarrow$
h_0	initial height	2.0 [m]	$\rightarrow$
v_0	initial velocity	6–9 [m/s]	9 [m/s]
m	mass of athlete	80 [kg]	$\rightarrow$
g	acceleration of gravity	9.8 [m/s^2]	$\rightarrow$
E	Young's modulus	70 [GPa]	$\rightarrow$
I	area moment of inertia	5 [cm^4]	$\rightarrow$
f_s	exerted force from the pole	-	$\rightarrow$
u	input bending moment	-	$\rightarrow$

TABLE II

SPECIFICATIONS OF PABRO.

parameter	value
mass	1.5 [kg]
entire size	220(L)-220(W)-280(H) [mm]
DOF	3 (active $\times$1 and passive $\times$2)
materials	ABS chassis, aluminum board
battery	GoldenPower A23S (12VDC)
control board	Arduino Uno R3
valve driver	self-development board (8ch on-off)
push switch	Omron V-1569-1A5 (SPDT)
tank	500 [ml] aluminum tank
regulator	pressure controller (PISCO RVUM4-4)
valve	CKD 4GA130-C6E2-3 (5 ports on-off)
air cylinder	SMC CDJ-2B16-75A

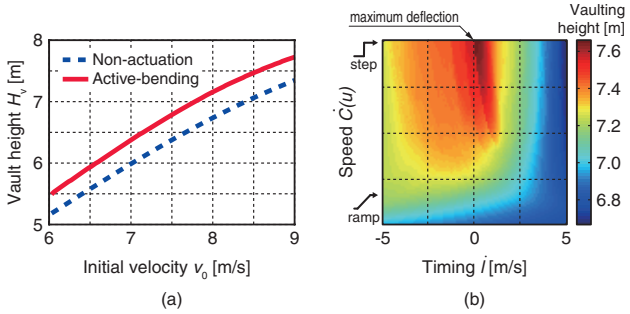

Fig. 3. (a) Vaulting height at each initial velocity. "Non-actuation" does not include pole actuation; "Active-bending" includes it. (b) Vaulting height map by the transition timing and the speed of change with end-support condition coefficient $C(u)$. The horizontal axis is the transition timing normalized by $\dot{l}$. When $\dot{C}(u)$ is large, the input bending moment is like a step input.

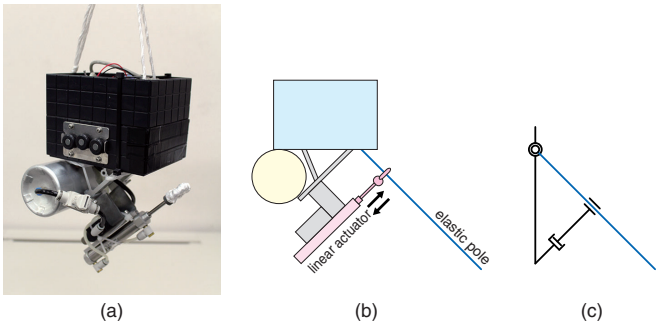

Fig. 4. Pole Active Bending RObot (PABRO). (a) Overview of PABRO. (b) Mechanical system of PABRO. (c) Degrees of freedom of PABRO. The robot has a linear actuator, a translational joint and a rotational joint.

B. Experiment 1: Active Bending Effect

In "Non-actuation", C is constant as $C = 1$. In "Active-bending", $C(u)$ is changed linearly from $C_1 = 0.8$ to $C_2 = 1.2$ centering around maximum deflecting timing. We changed the initial velocity from 6.0 m/s to 9.0 m/s. As a result, in "Active-bending", vaulting height H_V at each initial velocity was greater than in "Non-actuation" (Fig. 3 (a)). Consequently, the input bending moment improved the vaulting performance.

C. Experiment 2: How to Change the Input Bending Moment

Using TBM, we analyzed the effect of how $C(u)$ changes from C_1 to C_2. Vaulting height H_V on the map shows that H_V took a high value of around $\dot{l} = 0$, with a sharp increase in the area (Fig. 3 (b)). The point of $\dot{l} = 0$ is the point of minimum l, which is the timing at which the pole maximally deflects. Therefore, the robot is expected to change the direction of the bending moment like a step input at the time when the pole maximally deflects for improvement of the vaulting height.

IV. DEVELOPMENT OF POLE ACTIVE BENDING ROBOT

To verify active bending effect in the real world, we designed a robot that can actively apply the bending moment to the pole (Fig. 4 (a), Table II). The robot consisted of a chassis, an air tank and an air cylinder (Fig. 4 (b)). The robot required following functions.

1) The robot can apply the bending moment to the pole during "pole support phase."
2) The robot is lightweight.
3) External wires do not disturb the robot's vaulting.
4) The robot can maintain stable initial velocity.
5) The robot can correctly plant the pole into the pole plant box.

Therefore, we designed the robot as follows.

A. Active Bending Mechanism (for requirement (1))

Active bending mechanism is composed of a linear actuator with a rod, a translational joint and a rotational joint (Fig. 4 (c)). We attached an eyenut on the end of the rod and passed the pole through the hole of the eyenut to make a translational joint (Fig. 5 (a)). We perpendicularly pierced a pin through the end of the pole and inserted the pole into a hole in bottom of the chassis to make a rotational joint (Fig. 5 (b)). Actuation of the rod generates bending moment to the pole (Fig. 6). The rod extension bends the pole positively. When the rod is at the center, the rod has no effect on the pole. The rod shortening bends the pole negatively.

B. Pneumatically-driven and Self-contained System (for requirement (2) and (3))

To reduce the weight of the robot, we adopted pneumatically-driven system. To decrease disturbances, we designed the system as a self-contained system. Valve driver controls solenoid valves to supply air from air tank to air

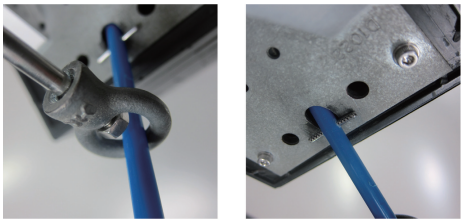

(a) translational joint (b) rotational joint

Fig. 5. Translational joint and rotational joint.

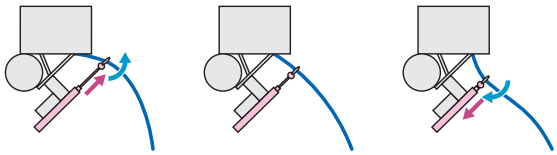

Fig. 6. Mechanism for generating active bending of PABRO. (a) Rod extension positively bends the pole. (b) When the rod is at the center, the rod has no effect to the pole. (c) Rod shortening negatively bends the pole.

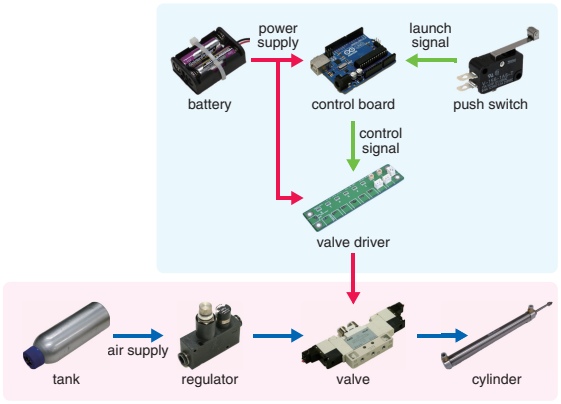

Fig. 7. System of PABRO. Blue area shows electrical system. Pink area shows air driven system.

cylinder (Fig. 7). Both electric resource and air resource were miniaturized and mounted on the robot. Therefore, external disturbances such as communication cable, power cable, air supply tube, and such were eliminated.

C. Pole Vaulting System (for requirement (4) and (5))

We developed pole vaulting system composed of a launcher and pole plant box connected to the launcher (Fig. 8 (a)). The launcher shoots the robot forward, and the robot plants the pole into the box (Fig. 8 (b)). Distance between the launcher and box is variable so we can adjust the distance for exact planting of the pole. The launcher generated stable initial robot velocity (Table III). The box was designed based on the pole vault rule book had no mechanical interface with the robot, so the pole behavior was not constrained along the sagittal plane.

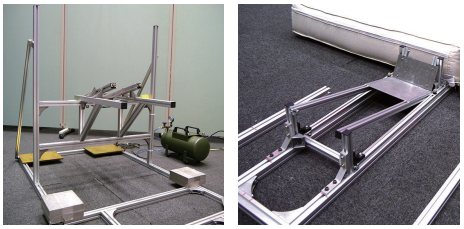

(a) launcher (b) pole plant box

Fig. 8. Experimental equipment.

TABLE III
LAUNCH TEST.

P_{in} [MPa]	V_{out} [m/s]	sample number
0.7	4.97 ± 0.03	5
0.8	5.19 ± 0.11	5
0.9	5.42 ± 0.06	5

A 1.5 kg weight was launched. The launch angle was set to 20 deg. P_{in} is the input air pressure. V_{out} is the mean shoot out velocity of the weight.

V. Robot Experiments

We specifically examined the advantages of the active bending motion. To compare them, we conducted the following experiments. First, we experimentally compared the vaulting height of the robot without active bending motion (Non-actuation) and the height of the robot with active bending motion (Active-bending). Next, in "Active-bending", we experimentally explored the vaulting performance, shifting the timing of change of the bending direction.

A. Experimental Setup

The whole pole vault system is shown in Fig. 9. The sequence of the pole vault experiment is the following.

(i) The robot is launched by the launcher (Fig. 8 (a)) to give the robot an initial velocity.
(ii) The robot plants the pole into the pole plant box (Fig. 8 (b)).
(iii) The robot hangs from the deflecting pole. In these experiments, robots actuate the pole in this phase.

Robot's motion commands are the following.

Non-actuation
Neutral ($T_{\text{PP}} \leq t \leq T_{\text{PR}}$)
Active-bending
Positive Bending ($T_{\text{PP}} \leq t \leq T_{\text{SW}}$)
Negative Bending ($T_{\text{SW}} < t \leq T_{\text{PR}}$)

Here, T_{PP} is the time when the robot plants the pole into the box. T_{SW} is the time when motion command changes from "Positive Bending" to "Negative Bending" and is an experimental parameter. T_{PR} is the time when the robot releases the pole.

Additionally, the robot had no feature to release the pole. Therefore, vaulting height H_{V} was defined as a maximum height of CoG in a projectile motion, assuming the position and velocity that the robot's CoG had at pole release timing (h_1, v_1 in Fig. 10) as an initial state (Eq. (4)). We defined

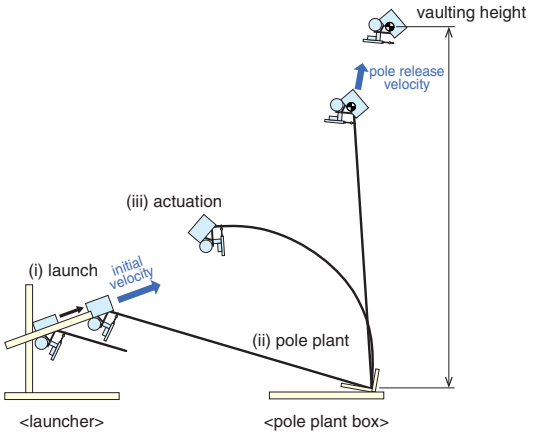

Fig. 9. Pole vault system.

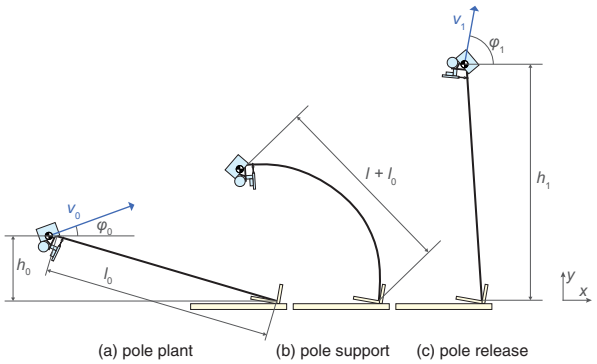

Fig. 10. Experimental parameters.

TABLE IV

PARAMETERS OF THE ROBOT EXPERIMENT.

parameter	description	value
m	mass of robot	1.5 [kg]
l_0	pole length	1.00 [m]
v_0	initial velocity	4.2 [m/s]
ϕ_0	angle of initial velocity	20 [deg]
h_0	initial height	0.55 [m]
v_1	velocity at T_{PR}	measured
ϕ_1	angle of velocity at T_{PR}	measured
h_1	height at T_{PR}	measured
$P_{\max}$	upper limit of air pressure	0.45 [MPa]

TABLE V

POLE SPECIFICATIONS.

parameter	value
name	Danpole Maru 65 Blue (UEXC)
Young's modulus	19.3 [GPa]
area moment of inertia	77.3 [mm^4]

TABLE VI

VAULTING HEIGHT OF THE POLE VAULT ROBOT.

parameter	Non-actuation	Active-bending	t-test's P
n	10	5	-
v_0 [m/s]	4.23 ± 0.08	4.18 ± 0.08	2.9×10^{-1}
H_{V} [m]	1.04 ± 0.01	1.19 ± 0.06	1.1×10^{-6}
H_{Re} [m]	1.03 ± 0.01	1.05 ± 0.01	6.6×10^{-3}
$\varepsilon_{\max}$ [%]	18.6 ± 1.1	25.7 ± 0.3	2.7×10^{-9}
$\dot{l}_{\max}$ [m/s]	0.66 ± 0.06	1.73 ± 0.34	1.9×10^{-7}
v_1 [m/s]	0.93 ± 0.33	1.88 ± 0.24	7.3×10^{-5}
ϕ_1 [deg]	16.2 ± 8.1	65.3 ± 8.2	5.6×10^{-8}
v_{1y} [m/s]	0.25 ± 0.17	1.60 ± 0.37	2.1×10^{-7}

"pole release timing" as the time when the pole absolutely re-straightens.

$$H_{\mathrm{V}} = h_1 + \frac{(v_1 \sin \phi_1)^2}{2g}. \tag{4}$$

Here, m denotes the robot mass, g stands for the acceleration of gravity, h_1 is the robot's CoG height, v_1 represents the robot's CoG velocity, and ϕ_1 is the elevation angle of the velocity at the pole release point.

We chose parameters based on simulation experiments (Table IV, Table V). Pole length: 1.00 m is the value which produced the highest vault in "Non-actuation" in the simulation. The robot movements were measured using a Vicon motion capture system (Vicon Motion Systems Ltd.), which captured the experiment at 120 Hz. The robot was controlled by an open-loop controller.

B. Experiment 1: Effect of Active Bending

To verify the effect of active bending, we compared the pole vaulting height of the robot without active bending (Non-actuation) and with active bending (Active-bending).

Results of the robot's pole vault experiment are shown in Fig. 11. The performance was improved by the active bending effect (see supplemental movie). In "Active-bending", the robot and pole succeeded in elevating from the box.

As a result, while vaulting height H_{V} is 1.04 ± 0.01 [m] in "Non-actuation", H_{V} is 1.19 ± 0.06 [m] in "Active-bending" (H_{V} in Table VI, Fig. 12 (a)). Each height had a significant difference (Student's t-test, $P = 1.1 \times 10^{-6}$). The difference in vaulting height ΔH_{V} between both vaulting heights was 0.15 [m]. The performance improved 14% when Active-bending was implemented. Furthermore, H_{Re} defined as the maximum CoG height of the robot in motion capture data also improved (H_{Re} in Table VI). For reference, $H_{\mathrm{l}} = 1.03$ [m] was a sum of the pole length and offset length of the robot's CoG from pole holding point.

To investigate the causes of improvement of vaulting height, we examined the robot trajectories (Fig. 12 (b)). In the positive bending phase, the pole in "Active-bending" was deflected 1.4 times more extremely than the pole in the "Non-actuation" condition ($\varepsilon_{\max}$ in Table VI).

$$\varepsilon_{\max} = \frac{\Delta l_{\max}}{l_0}. \tag{5}$$

Therefore, the pole accumulated greater elastic energy with "Active-bending". In the negative bending phase, the pole in "Active-bending" straightens 2.6 times more quickly than the pole in the "Non-actuation" ($\dot{l}_{\max}$ in Table VI).

$$\dot{l}_{\max} = \max\left(\dot{l}(t)\right). \tag{6}$$

Therefore, the robot received greater force from the pole. In

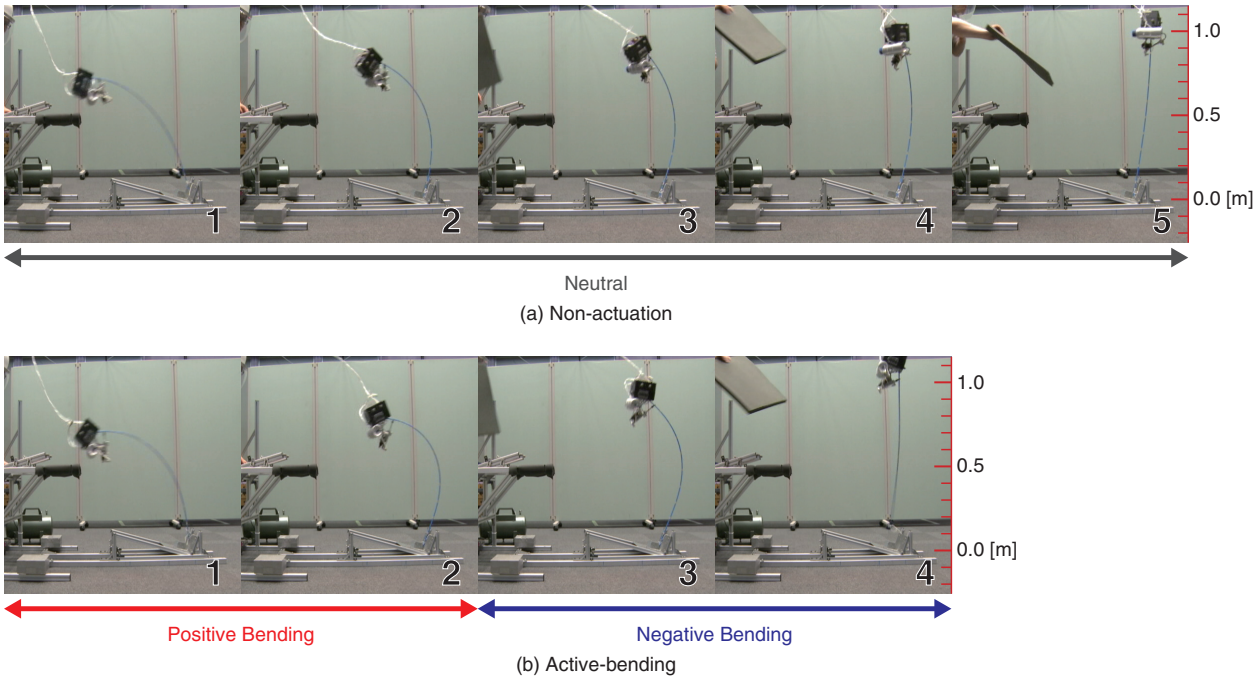

Fig. 11. Photographs of pole vault experiments. Time step is 1/6 [s].

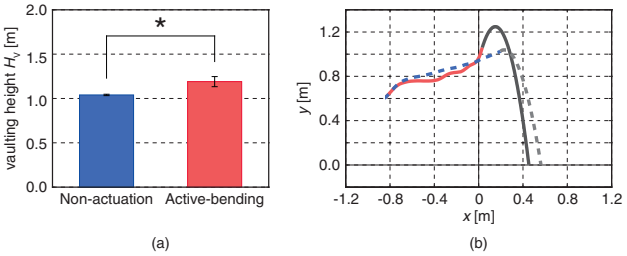

Fig. 12. Results of robot experiments. (a) Comparison of the vaulting height between "Non-actuation" and "Active-bending." The error bar shows the standard deviation. The vaulting height showed a significant difference between "Non-actuation" and "Active-bending" (Student's t-test, $P = 1.1 \times 10^{-6}$). (b) Trajectories of the robot's CoG. Blue line is the trajectory in "Non-actuation." Red line is the trajectory in "Active-Bending." Gray line is the estimated trajectory.

consequence, at the pole release timing, the robot in "Active-bending" had 2.0 times larger velocity than the robot in "Non-actuation" (v_1 in Table VI).

Moreover, vaulting angle in "Active-bending" was larger than in "Non-actuation" (ϕ_1 in Table VI). Therefore, vertical component of the velocity $\sin\phi_1$ in "Active-bending" was 3.3 times larger than in "Non-actuation." In consequence, although "Non-actuation" had little vertical velocity (0.25 ± 0.17 [m/s]), "Active-bending" had sufficient vertical velocity to upfly (1.60 ± 0.37 [m/s]).

In summary, increasing the vaulting velocity and verticalization of the vaulting angle improved vaulting height.

We estimated an energy rate between supply and consumption. The air cylinder stroked a half (Neutral $\rightarrow$ Positive Bending) and one (Positive Bending $\rightarrow$ Negative Bending) length of the cylinder. Therefore, we calculated the cylinder supply energy E_{sup} as the following equation.

$$E_{\mathrm{sup}} = \int_{V/2}^{V} P(V)dV + \int_{\mathrm{V}}^{0} P(V)dV \quad (7)$$

$$\leq P_{\max}\frac{\pi D^2}{4}L \times \frac{3}{2} = 10.2 \text{ [J]}. \quad (8)$$

Here, P represents the inner pressure of the cylinder, $P_{\max} = 0.45$ [MPa] is the available pressure of the air tank, $D = 16$ [mm] denotes the cylinder diameter, and $L = 75$ [mm] is the stroke of the cylinder. Therefore, the maximum increase of the vaulting height caused by cylinder actuation ΔH_{vsup} was estimated using the following equation.

$$\Delta H_{\mathrm{vsup}} = \frac{E_{\mathrm{sup}}}{mg} = 0.69 \text{ [m]}. \quad (9)$$

Here, m stands for the mass of the robot, g is the gravitational acceleration constant. ΔH_{V} is 0.15 [m], so at least more than 22% of the supplied energy was consumed for the increase of the vaulting height.

C. Experiment 2: Timing Effect in Switch of Bending Direction

To analyze the effect of the timing of bending direction change (switching from Positive Bending to Negative Bending), we experimented with some timing (Fig. 13 (a)). The vaulting height h_{V} had a peak value relative to the switching timing. The vaulting height trajectory was sharply pointed at the peak. Therefore, the timing was inferred as an important factor for improving the pole vaulting performance.

The timing to vault the highest was 125 ms later than the time when the pole was maximally deflected. Comparison to the simulation results shows that the best timing was shifted later.

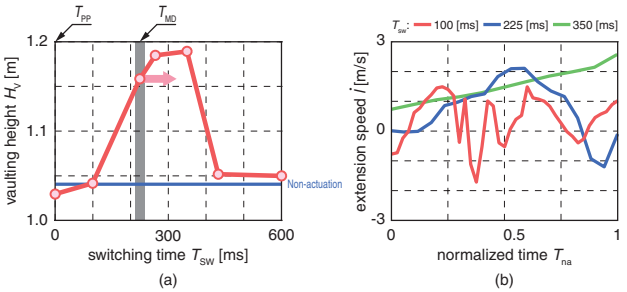

Fig. 13. (a) Vaulting height on some timing of the bending direction change. T_{SW} represents the time between pole planting and changing direction of bending moment. T_{MD} is the time when pole maximally deflect in keeping positive Bending. Blue line means the vaulting height H_V in the "Non-actuation". (b) Pole vibration related to T_{sw}. T_{na} is normalized time between T_{sw} and pole releasing. $\dot{l}$ shows differential of the segment length from the bottom end of the pole and the top end of it. In $T_{SW} = 350$ [ms], plot shows mean of 5 samples (same data in "Active-bending" in experiment 1). In other T_{SW}, plot shows 1 sample at each T_{SW}.

One possible reason was presence of inertia force [11]. Although we did not account for skipped the inertia force in simulation experiments, robot's switching motion generated inertia force during the real world experiment. If the robot switches bending direction early in the vaulting sequence, torque which stems from the inertia force prevents pole rising.

Another possible explanation was that a vibration decreased the vaulting height in early switching time. If the switching timing was early, the local extension near the top end of the pole was earlier than whole extension of it. Therefore, the pole had thumping vibration (Fig. 13 (b)). The earlier the timing was, the higher frequency the vibration had.

VI. DISCUSSION

We discuss an application of active bending theory for the robot using other elastic devices. We generalize the active bending theory for application to other systems.

(i) The robot actuates the elastic device while the robot contacts the environment through the elastic device.
(ii) Energy from the actuation changes the elastic property of the device.
(iii) The robot behavior is affected through the shift of elastic property.

Based on the result of this research, appropriate change of the elastic property improves the robot's locomotive performance.

We can apply the theory to the coil spring system, which is generally used as an elastic element.

(i) The robot twists the coil spring.
(ii) A change of the number of turns varies the spring constant.
(iii) The exerted force changes as a function of the spring constant.

For instance, when a one-legged hopping robot with a coil spring leg twists its body appropriately and quickly during the contacting duration, the robot can hop higher.

In pole vault, the long duration of the contact phase gives the robot adequate time to actuate. In other tasks, if the actuation time such as the control period and the following capability of the actuator is enough smaller than the length of the contact duration, we can also apply the theory to control various elastic devices. In this experiment (contacting duration: 700 [ms]), we improved the performance with the actuator whose actuation time was about 100 [ms/action]. Therefore, equipping the actuator with around 1/10 time ratio (actuation time per conduct duration), we will be able to apply the theory to other tasks.

VII. CONCLUSION

As described herein, we proposed an active bending theory in pole vaulting. We verified it through simulation and using a robot experiment. Results show that actuation of the robot, which was suspended from a pole, improves the pole vaulting performance. Increasing the vaulting velocity and verticalization of the vaulting angle improved vaulting height. The switching timing of the bending direction is an important factor in defining the performance. Emergence of the inertia force and the vibration shift the timing later in real world. We discussed the active actuation during the long contacting phase. The theory will be applied to the robot with other elastic devices.

ACKNOWLEDGMENT

We thank Yuko Hara for her valuable comments on the draft of the manuscript.

REFERENCES

[1] M. H. Raibert, *Legged robots that balance*. MIT press Cambridge, MA, 1986, vol. 3.
[2] M. Raibert, M. Chepponis, and H. Brown Jr, "Running on four legs as though they were one," *IEEE Journal of Robotics and Automation*, vol. 2, no. 2, pp. 70–82, 1986.
[3] S.-H. Hyon and T. Mita, "Development of a biologically inspired hopping robot," in *IEEE International Conference on Robotics and Automation (ICRA)*, vol. 4, 2002, pp. 3984–3991.
[4] M. Ahmadi and M. Buehler, "Controlled passive dynamic running experiments with the arl-monopod ii," *IEEE Transactions on Robotics*, vol. 22, no. 5, pp. 974–986, 2006.
[5] B. Brown and G. Zeglin, "The bow leg hopping robot," in *IEEE International Conference on Robotics and Automation (ICRA)*, vol. 1, 1998, pp. 781–786.
[6] J. Frère, B. Göpfert, J. Slawinski, and C. Tourny-Chollet, "Effect of the upper limbs muscles activity on the mechanical energy gain in pole vaulting," *Journal of Electromyography and Kinesiology*, vol. 22, no. 2, pp. 207–214, 2012.
[7] P. M. McGinnis and L. A. Bergman, "An inverse dynamic analysis of the pole vault," *International Journal of Sport Biomechanics*, vol. 2, no. 3, pp. 186–201, 1987.
[8] T. Fukushima, S. Nishikawa, K. Tanaka, and Y. Kuniyoshi, "Transitional buckling model for active bending effect in pole vault," in *6th International Symposium on Adaptive Motion of Animals and Machines (AMAM)*, 2013.
[9] N. P. Linthorne, "Energy loss in the pole vault take-off and the advantage of the flexible pole," *Sports Engineering*, vol. 3, no. 4, pp. 205–218, 2001.
[10] G. Liu, S.-K. Nguang, and Y. Zhang, "Pole vault performance for anthropometric variability via a dynamical optimal control model," *Journal of Biomechanics*, vol. 44, no. 3, pp. 436–441, 2011.
[11] S. Nishikawa, T. Fukushima, and Y. Kuniyoshi, "Effective timing of swing-up motion by a pole-vaulting robot," in *16th International Conference on Advanced Robotics (ICAR)*, 2013.